Journal of Physics and Chemistry of Solids 71 (2010) 1694–1701

Contents lists available at ScienceDirect

Journal of Physics and Chemistry of Solids

journal homepage: www.elsevier.com/locate/jpcs

Kondo behaviour of the solid solution $(Ce_{1-x}La_x)PtGa$

F.C. Ragel [a,b,*], P. de V. du Plessis [a,b], A.M. Strydom [a]

[a] Physics Department, University of Johannesburg, P.O. Box 524, Aucklandpark 2006, South Africa
[b] School of Physics, University of the Witwatersrand, Private Bag 3, PO WITS 2050, Johannesburg, South Africa

ARTICLE INFO

Article history:
Received 25 January 2010
Received in revised form
12 June 2010
Accepted 16 August 2010

Keywords:
A. Magnetic materials
D. Magnetic properties
D. Specific heat
D. Transport properties

ABSTRACT

The solid solution $(Ce_{1-x}La_x)PtGa$ has been studied through X-ray diffraction, magnetization ($\sigma(B)$), magnetic susceptibility ($\chi(T)$), electrical resistivity ($\rho(T)$), magnetoresistivity (MR) and heat capacity ($C_P(T)$) measurements. The Néel temperature ($T_N=3.3$ K) for CePtGa is lowered upon La substitution as observed from $\chi(T)$ and $\rho(T)$ measurements. The Kondo temperature T_K as calculated from MR measurements is comparable to T_N and also decreases with La substitution. The volume dependence of T_K is in accordance with the compressible Kondo lattice model and a Doniach diagram of the results is presented. $C_P(T)$ measurements are presented for CePtGa, $Ce_{0.2}La_{0.8}PtGa$ and LaPtGa and the results are discussed in terms of the electronic and magnetic properties. Other features of interest are anomalies in $\rho(T)$ and $C_P(T)$ due to crystalline electric field effects and metamagnetism as observed in $\sigma(B)$ studies for samples with $0 \le x \le 0.3$.

1. Introduction

The antiferromagnetic (AF) Kondo compound CePtGa has been studied by several authors on polycrystalline [1–4] and single crystal [4,5] samples. The compound has the orthorhombic TiNiSi-type structure (space group *Pnma*). It orders at a Néel temperature $T \sim 3.3$ K [6,7]. Experimental studies include electrical resistivity ($\rho(T)$) measurements at ambient [5–7] and hydrostatic pressure [2], susceptibility ($\chi(T)$) studies [5,7], heat capacity (C_P(T)) measurements [4], magnetoresistance (MR) studies [3,7] and inelastic neutron scattering studies [3]. The latter measurements suggest a Kondo temperature $T_K=2.2$ K for CePtGa. The closeness of T_K and T_N makes the system ideal for studying the interplay between the Kondo and RKKY interactions, and from the results of $\chi(T)$, $\rho(T)$ and MR measurements on CePtGa, $Ce(Pt_{1-y}Ni_y)Ga$ and $CePt(Ga_{1-z}Al_z)$ solid solutions we have presented a Doniach diagram of the volume dependence of T_K and T_N [6,7]. The possible existence in the $Ce(Pt_{1-y}Ni_y)Ga$ solid solution of a quantum critical point (QCP) near $y=0.38$ has been reported previously [7]. In this work the stability of the Kondo effect with respect to La dilution on the f-electron site in CePtGa is investigated through magnetization $\sigma(B)$, $\chi(T)$, $\rho(T)$, MR and $C_P(T)$ measurements. The compound LaPtGa also forms in the orthorhombic TiNiSi-type structure [8] thus enabling a study of the complete range of solid solutions $(Ce_{1-x}La_x)PtGa$ $(0 \le x \le 1)$. The present results for the solid solutions $(Ce_{1-x}La_x)PtGa$ are interrelated with those obtained previously for $Ce(Pt_{1-y}Ni_y)Ga$ [7].

2. Experimental details

Polycrystalline samples of $(Ce_{1-x}La_x)PtGa$ were prepared by arc-melting on a water-cooled copper hearth stoichiometric amounts of the constituent elements but augmenting the starting composition by the addition of 2% Ga to compensate for the possible loss of this low-melting temperature element as described in [7]. Each sample was arc-melted three times with intermittent overturning of the ingot in a titanium gettered ultra-pure argon gas atmosphere. The purities in wt% of the materials used were Ce: 99.98, La: 99.99, Pt: 99.97 and Ga: 99.9999. The weight-loss after melting ranged from 0.2–0.5% of the total sample mass and deviation of Ga content from stoichiometry is estimated as within $\pm 1.5\%$ based on the assumption that all of the weight loss is due to Ga evaporation.

Room-temperature powder X-ray diffraction (XRD) analyses of the specimens were made in order to establish their crystal structure, confirm their single-phase character and determine their lattice parameters. No evidence of any parasitic phases was observed within the accuracy of our diffractograms. WinPLOTR beta version by Laboratoire Leon Brillouin (CEA-CNRS) were used to resolve Bragg reflections of powder diffraction data for $10^\circ < 2\theta < 85^\circ$; $\lambda(CuK_\alpha=1.54056$ Å). Miller indexing of Bragg reflections were done for the orthorhombic system using the REFLEX software with reflection conditions $0kl$: $k+l=2n$; $0k0$:

* Corresponding author. Permanent address: Department of Physical Sciences, South Eastern University, Oluvil, Sri Lanka.
Tel: +94 714402270; fax: +94 672260932.
E-mail addresses: chalmusragel@seu.ac.lk, chalmusragel@gmail.com (F.C. Ragel).

0022-3697/$ - see front matter © 2010 Elsevier Ltd. All rights reserved.
doi:10.1016/j.jpcs.2010.08.010

$k=2n$; $00l$: $l=2n$; $hk0$: $h=2n$; and $h00$: $h=2n$ for the space group *Pnma*. Lattice parameters were calculated from the program UnitCell [9] for 32 well-resolved reflections refined for the orthorhombic system by minimising the sum of squares of residuals in 2θ.

Measurements of $\rho(T)$ were performed on all alloys using a standard four-probe dc method between 300 and 4 K. For some selected samples $\rho(T)$ and MR measurements were performed down to 2 K using a 9 T magnet of the physical property measurement system (PPMS) supplied by *Quantum Design*. Samples for $\rho(T)$ studies were bar shaped and of typical dimensions $6\times1\times1$ mm^3.

Magnetization and susceptibility measurements were obtained using the vibrating sample magnetometer option of the PPMS with sample temperatures varied and controlled in the range 2–400 K. Dimensions of typical samples used in these studies were $3\times1\times1$ mm^3 and the magnetic field B was applied along the long axis of the bar. It is noted that we use B for $\mu_0 H$ throughout this paper for the sake of simplicity. Heat capacity measurements were performed with the PPMS on some selected samples using a relaxation technique.

3. Results and discussion

3.1. X-ray diffraction analysis

The room-temperature orthorhombic lattice parameters a, b and c and unit-cell volume V of the compositions $0\le x\le1$ of the solid solutions $(Ce_{1-x}La_x)PtGa$ are given in Table 1 and its concentration dependence is illustrated in Fig. 1. Our room-temperature lattice parameters are consistent with the values $a=0.7157(2)$, $b=0.4487(1)$ and $c=0.7768(2)$ nm reported for CePtGa and $a=0.7263(2)$, $b=0.4522(1)$ and $c=0.7808(2)$ nm reported for LaPtGa in an earlier study [8].

The dashed lines in Fig. 1 represents least-squares (LSQ) fits to the data and illustrate that Vegard's rule is followed within the error bars of most of the data points over the complete range of x for this system. The notable exception is for the $x=0.6$ sample where the data and associated error bars falls just outside the LSQ line for the a and b axes. It is nevertheless noted that the linear LSQ fit for the unit cell volume $V(x)$ conforms very well with Vegard's rule for all values of x. This $V(x)$ result is used in Section 3.6 to discuss the volume dependence of T_N and T_K for the $(Ce_{1-x}La_x)PtGa$ system.

3.2. Zero-field resistivity measurements

Results of $\rho(T)$ measured on selected $(Ce_{1-x}La_x)PtGa$ samples down to 4 or 2 K and for the parent compound down to 300 mK are depicted in Fig. 2. Values of $\rho(T)$ initially decrease for all samples with a decrease in temperature and go through a minimum round about 25 K for Ce containing samples. With further reduction in temperature, $\rho(T)$ increases for these samples

Table 1
The orthorhombic lattice parameters a, b and c and the unit-cell volume V of the solid solutions $(Ce_{1-x}La_x)PtGa$. The figures in parentheses are standard deviations.

x	a (nm)	b (nm)	c (nm)	V (nm^3)
0.0	0.7162(2)	0.4488(1)	0.7759(2)	0.2494(1)
0.2	0.7183(2)	0.4493(2)	0.7765(3)	0.2506(1)
0.4	0.7198(2)	0.4500(1)	0.7782(2)	0.2521(1)
0.6	0.7215(2)	0.4511(2)	0.7789(2)	0.2535(1)
0.8	0.7242(2)	0.4515(1)	0.7803(2)	0.2552(1)
1.0	0.7266(3)	0.4523(2)	0.7812(2)	0.2567(1)

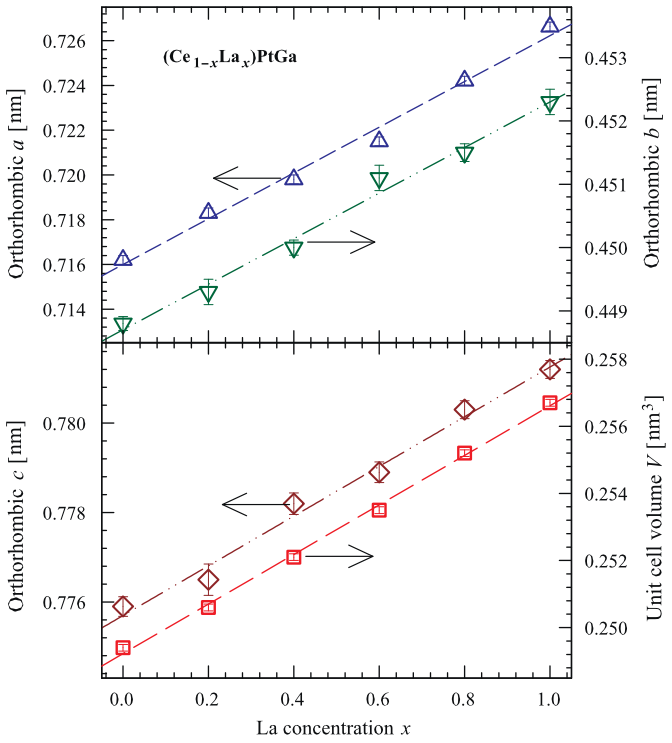

Fig. 1. The orthorhombic lattice parameters a, b and c and the unit cell volume V as a function of La concentration x in the solid solution $(Ce_{1-x}La_x)PtGa$.

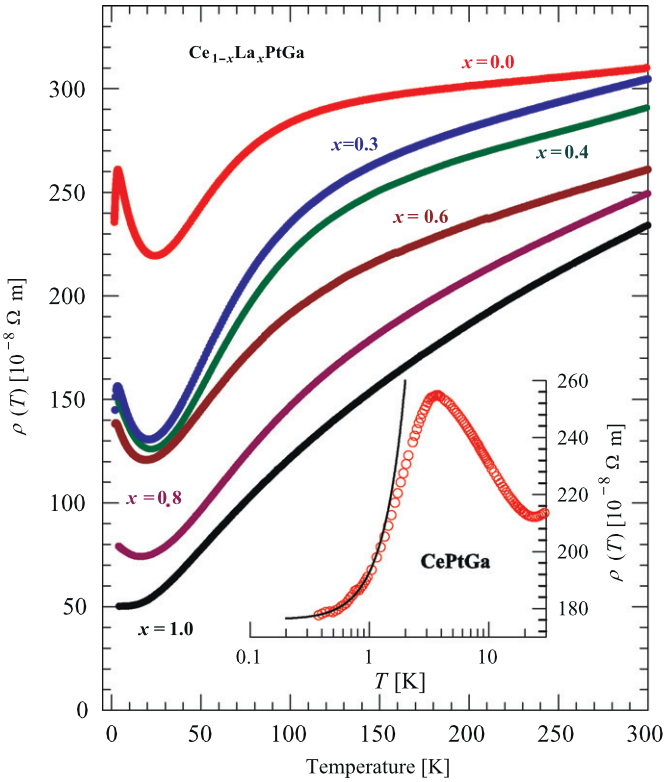

Fig. 2. The temperature dependence of the resistivity $\rho(T)$ of $(Ce_{1-x}La_x)PtGa$ samples. The solid line in the inset shows a fit of a spin-wave expression (1) for $\rho(T)$ to the low-temperature data for CePtGa.

and for the $x=0$, 0.3 and 0.6 samples shows a small peak at low temperatures (also see Fig. 3 for more detail). As follows in Section 3.3 from the $\chi(T)$ results, the peaks of $\rho(T)$ for the $x=0.0$

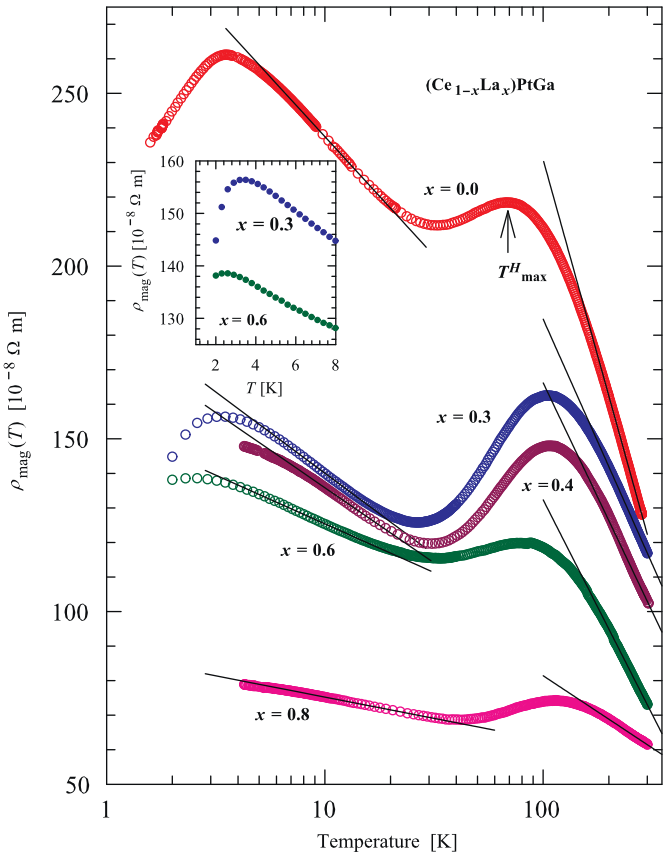

Fig. 3. The Kondo resistivity found by correcting for the phonon resistivity as $\rho_{mag}(T)=\rho_x(T)-[\rho_{x=1}(T)-\rho_{x=1}(0)]$. A temperature dependence of $(-\ln T)$ is observed in two temperature regions.

and 0.3 samples indicate antiferromagnetic ordering. Since the $\chi(T)$ results do not show a peak for the $x=0.6$ sample, the low-temperature peak in $\rho(T)$ for this sample (see also Fig. 3) should be of Kondo origin. The $\rho(T)$ results at low temperatures for the parent compound are shown in the inset to Fig. 2. For antiferromagnets $\rho(T)$ may be taken as [10]

$$\rho(T)=\rho(0)+b\Delta^2\sqrt{\frac{T}{\Delta}}\exp(-\Delta/T)\left[1+\frac{2}{3}\left(\frac{T}{\Delta}\right)+\frac{2}{15}\left(\frac{T}{\Delta}\right)^2\right] \quad (1)$$

where $\rho(0)$ is the temperature-independent residual resistivity, b is a constant that characterizes the particular AF material and Δ is the gap in the spin-wave spectrum as described by a dispersion relation $\varepsilon_k=\sqrt{\Delta^2+Dk^2}$ with D the spin-wave stiffness. A LSQ fit of Eq. (1) against the experimental data at low temperatures is presented as a solid line in the inset and yields fit parameters $\rho(0)=176(3)\times10^{-8}\,\Omega\,m$, $b=20(2)\times10^{-8}\,\Omega\,m\,K^{-2}$ and $\Delta=0.6(1)$ K.

In Fig. 3 the Kondo resistivity $\rho_{mag}(T)$ of the parent compound and of the $x=0.3$, 0.4, 0.6 and 0.8 samples as obtained by subtracting the phonon contribution is given: $\rho_{mag}(T)=\rho_x(T)-[\rho_{x=1}(T)-\rho_{x=1}(0)]$. All Ce containing samples exhibit a $(-\ln T)$ dependence of $\rho_{mag}(T)$ in two different temperature regimes. This is reminiscent of the behaviour of this quantity for several Ce systems, e.g. Ce_2T_2In (T=Cu, Au or Pd) [11], $Ce_2Rh_3Ge_5$, $Ce_2Ir_3Ge_5$ [12] and $Ce_2Ni_2Ge_5$ [13]. The origin of this behaviour is due to the combined effect of Kondo and crystal–electric-field interactions as treated by Cornut and Coqblin [14]. LSQ fits of

$$\rho_{mag}(T)=A-C_K\ln T \quad (2)$$

to the experimental data as indicated in Fig. 3 yield values in lower and higher crystal field (CF) levels as tabulated in Table 2.

3.3. Magnetization and susceptibility

Results of magnetization $\sigma(B)$ measurements for the $(Ce_{1-x}La_x)$PtGa system with $0\le x\le0.8$, are depicted in Fig. 4a for the 2 K isotherms. Metamagnetic behaviour is observed for samples with

Table 2
A^L, C_K^L (in the lower CF level) and A^H, C_K^H (in the higher CF level) values extracted from LSQ fits of Eq. (2) as shown by solid lines in Fig. 3 in the two temperature regimes.

x	A^L ($10^{-8}\Omega$ m)	C_K^L ($10^{-8}\Omega$ m)	A^H ($10^{-8}\Omega$ m)	C_K^H ($10^{-8}\Omega$ m)
0.0	306.4(2)	29.9(1)	685.4(4)	98.71(7)
0.3	187.1(1)	20.41(6)	468.5(4)	61.63(7)
0.4	179.3(2)	18.89(8)	431(1)	57.6(2)
0.6	153.6(1)	12.25(6)	381.0(5)	54.98(9)
0.8	87.56(9)	5.35(3)	165.1(3)	18.17(6)

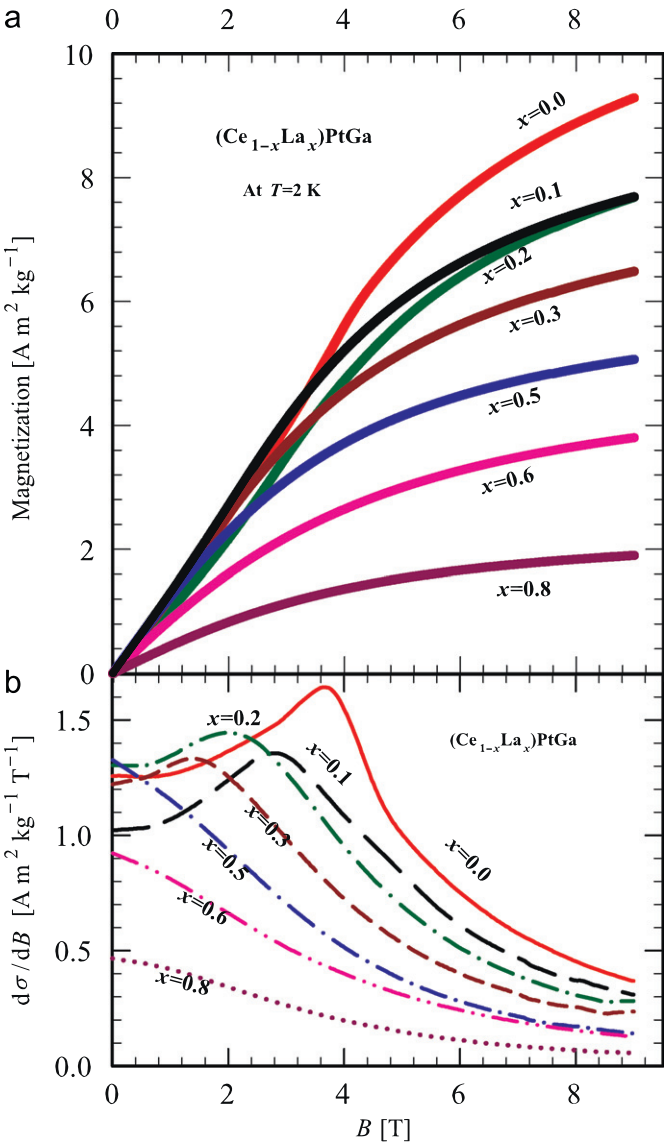

Fig. 4. (a) Isotherm magnetization results taken at 2 K for samples with $0\le x\le0.8$. (b) Curves of $d\sigma/dB$ in which the maxima indicate the fields where metamagnetic transitions take place.

$0 \le x \le 0.3$ at critical fields ranging from 3.7 T for $x=0$ to 1.4 T for $x=0.3$ as indicated by the peak values in $d\sigma/dB$ shown in Fig. 4b. For isotherms above 2 K (not shown) the curvature progressively decreases with increase in temperature and the curves become completely linear for the 10 K isotherms of all samples. We did not pursue the possible temperature dependence of the critical fields in view of the limited temperature region in the AF state for which measurements could be taken.

$\chi(T)$ results taken in $B=0.1$ T, which are for all samples and at all temperatures in the linear region of the $\sigma(B)$ curves, are shown in Fig. 5. The maxima that appear for samples with $0 \le x \le 0.3$ indicate AF ordering and are used to obtain the T_N values given in Table 3 and discussed in Section 3.6.

Plots of the inverse susceptibility $\chi^{-1}(T)$ are depicted in Fig. 6. The various data sets exhibit Curié–Weiss behaviour

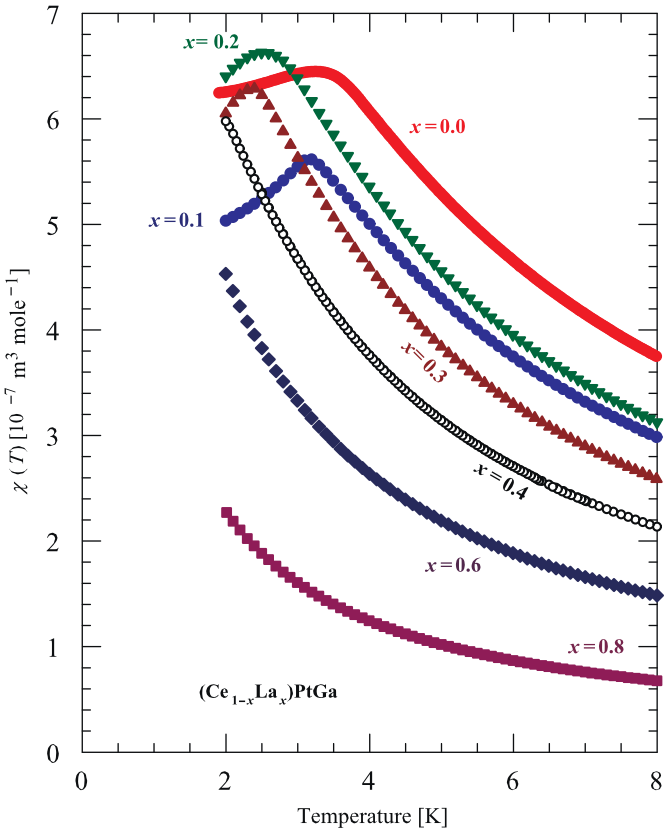

Fig. 5. The temperature dependence of the susceptibility $\chi(T)$ of the $(Ce_{1-x}La_x)PtGa$ samples in a 0.1 T field.

Table 3
The Weiss constant θ_P and effective magnetic moment μ_{eff} as obtained from LSQ fits of the Curie–Weiss relation to the $\chi^{-1}(T)$ data of Fig. 6. Error assignments are indicated by either the numbers given in brackets in the columns for $-\theta_P$ and μ_{eff} or in the columns for $\Delta(-\theta_P)$ and $\Delta(\mu_{eff})$, as described in the text. T_N values as obtained from the maxima in $\chi(T)$ shown in Fig. 5 are also given.

x	$-\theta_P$ (K)	μ_{eff} (μ_B/Ce)	$\Delta(-\theta_P)$ (K)	$\Delta(\mu_{eff})$ (μ_B/Ce)	T_N (K)
0.0	58.4(1)	2.508(2)	1.1	0.004	3.25
0.1	63.6(1)	2.427(3)	1.3	0.004	3.15
0.2	55.5(1)	2.488(2)	0.8	0.003	2.50
0.3	55.4(1)	2.445(2)	0.4	0.001	2.35
0.4	65.7(1)	2.562(3)	1.4	0.005	–
0.5	53.6(1)	2.516(4)	0.8	0.003	–
0.6	88.2(2)	2.786(7)	6.2	0.021	–
0.8	59.8(2)	2.511(8)	1.8	0.006	–

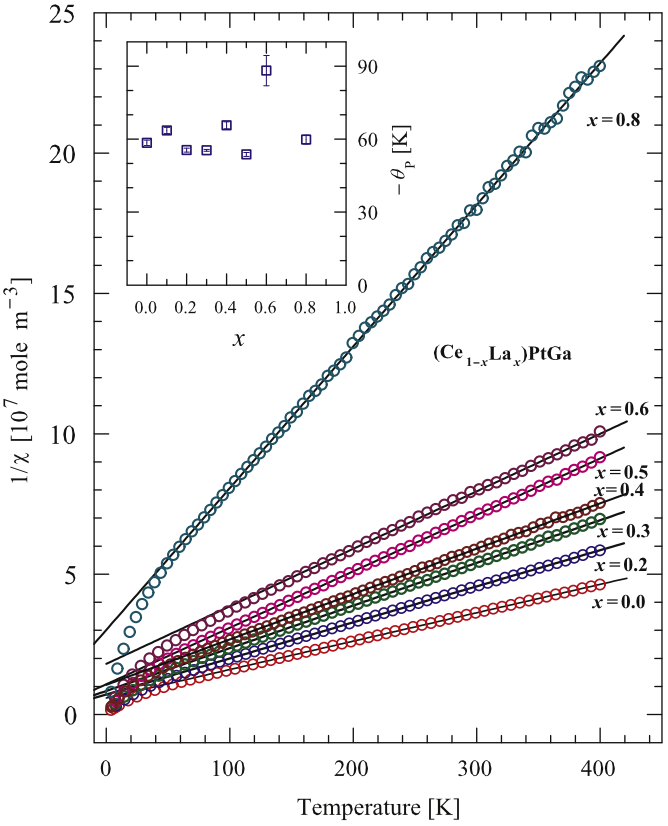

Fig. 6. Inverse magnetic susceptibility $\chi^{-1}(T)$ vs temperature for the $(Ce_{1-x}La_x)PtGa$ system illustrating Curie–Weiss behaviour (solid lines). The inset gives the concentration dependence of $-\theta_P$, where θ_P is the Weiss constant.

$\chi^{-1}(T)=(T-\theta_P)/C$ over most of the temperature range. Here $C=N_A\mu_{eff}^2/3\,k_B$ (N_A is Avogadro's number and k_B is Boltzmann's constant) for CePtGa, but assuming that the paramagnetic susceptibility behaves as a single-ion property, a scaling of the observed $\Delta T/\Delta\chi^{-1}=C$ with a factor of $(1-x)^{-1}$ needs to be made for the La containing samples in order to calculate μ_{eff}. LSQ fits of the Curié–Weiss relation to the experimental data in the temperature range 400 – 150 K are shown as solid lines in Fig. 6. These yield values of $-\theta_P$ and by employing the abovementioned scaling also of μ_{eff}. Values of $-\theta_P$ and of μ_{eff} for the different solid solutions of $(Ce_{1-x}La_x)PtGa$ are listed in Table 3 and the $-\theta_P$ values are depicted in the inset to Fig. 6. It is noted that the errors quoted in brackets in the listing of $-\theta_P$ and μ_{eff} values are obtained from the LSQ linear fits through the data points for the chosen temperature range 400 – 150 K. These errors are typical of the order of 0.1% for μ_{eff} and 0.15% for $-\theta_P$ which is small. Using however LSQ analyses for a different temperature range 400 – 100 K decreased both $-\theta_P$ and μ_{eff}, while using a range 400 – 200 K increased both these parameters from the values calculated for the 400 – 150 K range. Defining the difference in parameter values obtained for these two new ranges of fit as $2\Delta(-\theta_P)$ and $2\Delta(\mu_{eff})$ one associates the effect of varying the range of fit with an arbitrary amount $\pm\Delta(-\theta_P)$ and $\pm\Delta(\mu_{eff})$. Values of these error assignments are given in Table 3 and are for $-\theta_P$ an order of magnitude larger than the errors found directly through the LSQ fit procedure. These $\Delta(-\theta_P)$ values are used in the inset of $-\theta_P$ values in Fig. 6 and could be regarded as an upper limit of the errors associated with our results. The observed μ_{eff} values may be compared with the free Ce^{3+} ion value of 2.54 μ_B and are in fair agreement with this for all compositions except for the $x=0.6$ sample which show a distinctly larger value. This composition yield $-\theta_P=88.2\pm6.2$ which again is larger than the

$-\theta_P$ values observed for the other samples. These values are scattered around 60 K without showing any distinct pattern with x. It is also noted that larger errors in $-\theta_P$ and μ_{eff} are associated with the $x=0.6$ sample reflecting a poorer fit to the Curié–Weiss relation for this sample compared to the results for the other $(Ce_{1-x}La_x)PtGa$ solid solutions.

3.4. Magnetoresistivity

Magnetoresistance isotherms for the $x=0$, 0.3 and 0.6 samples are used in this section to extract their Kondo temperatures. A typical example of the results is shown in Fig. 7 for $Ce_{0.7}La_{0.3}PtGa$. The negative magnetoresistance is typical of a Kondo system and can be described by the Bethe Ansatz calculations of the Coqblin–Schrieffer model as formulated by Schlottmann [15]

$$\frac{\rho(B)}{\rho(0)} = \left[\frac{1}{2j+1}\sin^2\left(\frac{\pi n_f}{2j+1}\right)\sum_{\ell=0}^{2j}\sin^{-2}(\pi n_\ell)\right]^{-1} \quad (3)$$

Inelastic neutron scattering experiments on CePtGa show two well-defined crystal field levels at 209 and 413 K which are well separated from the ground state doublet and therefore these samples may be considered as a $j=1/2$ Ce impurity system at low temperatures. LSQ fits for the $j=1/2$ case of Eq. (3) to the experimental data are given as solid lines in Fig. 7. It is noted that Eq. (3) gives an excellent fit to the data for all fields up to 9 T for isotherms at 7 K and higher temperatures. However, for the lower temperature isotherms the data at high fields deviate from Eq. (3)

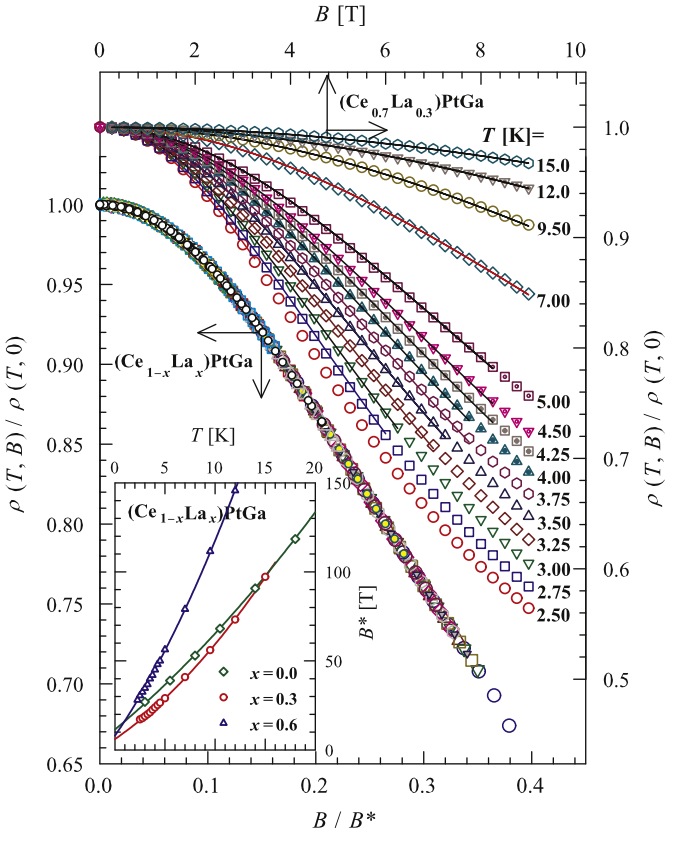

Fig. 7. The magnetic field dependence of electrical resistivity at a number of sample temperatures for the sample $(Ce_{0.7}La_{0.3})PtGa$. The solid curves in the main figure are LSQ fits of the Bethe Ansatz theory of magnetoresistance (Eq. (3)) to the experimental data. The inset shows the temperature variation of the characteristic field $B^*(T)$, and the line is a LSQ fit of Eq. (4) to the B^* values. Also shown as a single data curve for the $x=0$, 0.3 and 0.6 samples is the universal scaling of $\rho(T,B)/\rho(T,0)$ vs B/B^*.

and the fits are performed for these temperatures within a reduced field region as indicated by the solid lines in Fig. 7. The exact solutions for $j=1/2$ in the Schlottmann analysis indicate that the MR is determined by a single parameter B^*. A linear temperature dependence of B^* was proposed by Batlogg et al. [16] and found to be an appropriate description in MR studies of many Kondo systems for Ce or U diluted and for some stoichiometric compounds (see for instance [3,17]). Results of detailed measurements as shown in the inset to Fig. 7 indicate a deviation from linearity for the present system for which $B^*(T)$ is rather described by

$$B^*(T) = B^*(0) + c_1 T + c_2 T^2 \quad (4)$$

LSQ fits of Eq. (4) to the $B^*(T)$ values for respectively the samples with $x=0$, 0.3 and 0.6 enable evaluation of the magnetic moment of the Kondo ion μ_K from $\lim_{T\to 0}\left(\frac{dB^*}{dT}\right) = c_1 = \frac{k_B}{g\mu_K}$ and of T_K from $B^*(0) = \frac{k_B T_K}{g\mu_K}$ as found from extrapolation using Eq. (4). Values of T_K and μ_K are given in Table 4. Also shown in Fig. 7 is the excellent universal scaling obtained for $\rho(T,B)/\rho(T,0)$ against B/B^* for the $x=0$, 0.3 and 0.6 samples. The values obtained for μ_K are appreciably less than the μ_{eff} values in Table 3 deduced from the paramagnetic $\chi(T)$. The variation of T_K with x is discussed in Section 3.6.

3.5. Heat capacity

Measurements of the heat capacity C_P of CePtGa, $(Ce_{0.2}La_{0.8})PtGa$ and LaPtGa are depicted in Fig. 8 in the C_P/T vs T^2 presentation and fitted to the conventional equation for the heat capacity C_P of a metal at low temperatures

$$C_P/T = \gamma_0 + \beta T^2 \quad (5)$$

with γ_0 and β referring, respectively, to the electronic and phonon contributions. For the reference compound LaPtGa, the data conform to Eq. (5) down to low temperatures, with a small value of the electronic contribution to C_P as is to be expected, $\gamma_0=3.5$ mJ mol^{-1} K^{-2}. Values of γ_0 and β as obtained from LSQ fits of Eq. (5) to the experimental data are given in Table 5. It is observed that the γ_0 values of the Ce containing samples are appreciably enhanced compared to that of the reference compound. Also given in Table 5 are values of the Debye temperature θ_D for the different samples obtained from the relation $\theta_D = (12\pi^4 nR/5\beta)^{1/3}$ where R is the gas constant and n is the number of atoms in a formula unit.

As seen in the inset to Fig. 8, a peak in C_P/T occurs for CePtGa in the AF region at a temperature of 2.6 K which is somewhat below T_N. Assuming that the phonon contribution C_P^{ph} to the heat capacity of LaPtGa is a good approximation of C_P^{ph} in CePtGa, the non-lattice contribution was extracted in order to give $C_P^{mag}(x=0) = C_P(x=0) - C_P(x=1)$, where the last term in the expression also include the small contribution $C_P^{el} = \gamma_0 T$ of LaPtGa. The $C_P^{mag}(T)$ of CePtGa as obtained by the subtraction is used to calculate the temperature dependence of the magnetic entropy S^{mag} by integrating C_P^{mag}/T. Both $C_P^{mag}(T)$ and $S^{mag}(T)$ are plotted in

Table 4
Values of Kondo temperature T_K and the magnetic moment of the Kondo ion μ_K as obtained from fits of Eqs. (3) and (4) to the magnetoresistance data of the $(Ce_{1-x}La_x)PtGa$ samples.

x	T_K (K)	μ_K (μ_B)
0.0	2.4(3)	0.159(6)
0.3	1.6(1)	0.192(6)
0.6	1.0(1)	0.091(3)

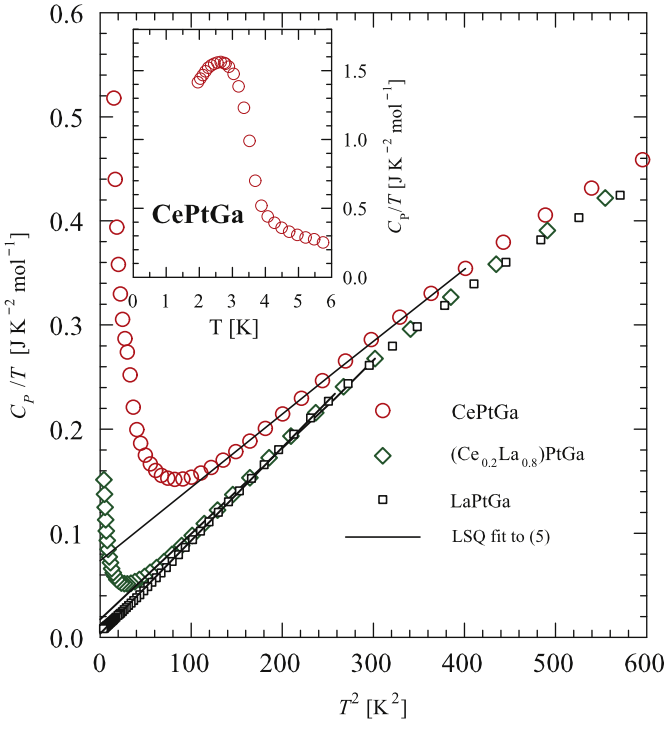

Fig. 8. C_P/T dependence on T^2 of $x=0.0$, 0.8 and 1.0 samples of the solid solution $(Ce_{1-x}La_x)PtGa$. The inset shows the low-temperature C_P/T dependence on T for CePtGa.

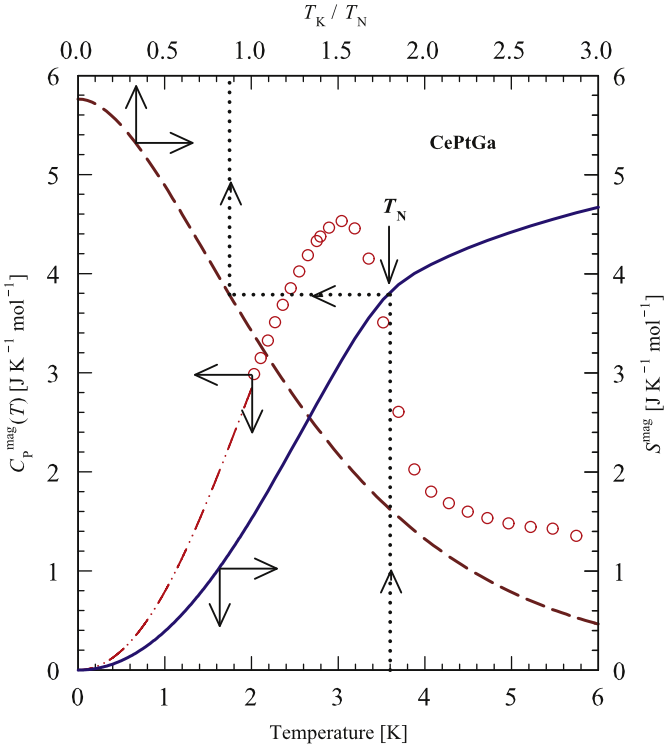

Fig. 9. Plot of $C_P^{mag}(T)=C_P(x=0)-C_P(x=1)$ and $S^{mag}(T)$ obtained by integrating C_P^{mag}/T. The quantity $S^{mag}(T_K/T_N)$ as obtained from Eq. (6) is indicated by a dashed line. The dotted lines show correspondence to $S^{mag}(T_N=3.6\ K)=S^{mag}(T_K/3.6\ K)$.

Table 5
Values of γ_0 and β obtained from fits of Eq. (5) in Fig. 8, as well as the Debye temperature θ_D.

Alloy	γ_0 (mJ mol^{-1} K^{-2})	β (mJ mol^{-1} K^{-4})	θ_D (K)
CePtGa	74(1)	0.704(4)	202(1)
$(Ce_{0.2}La_{0.8})PtGa$	10(2)	0.83(1)	192(2)
LaPtGa	3.5(2)	0.90(1)	186(1)

Fig. 9. The change in curvature of $S^{mag}(T)$ indicated by an arrow is associated with the onset of AF ordering at $T_N^{S(mag)}=3.6$ K which is slightly higher than $T_N^{\chi}=3.3$ K obtained by $\chi(T)$ measurements.

The magnetic entropy of a Kondo lattice has the form [18]

$$S(T_K/T_N)=R\ln[1+\exp(-T_K/T_N)] +R(T_K/T_N)\exp(-T_K/T_N)/[1+\exp(-T_K/T_N)] \quad (6)$$

and this relationship is plotted by a dashed line in Fig. 9. The dotted lines in the figure correspond to $S(T_N=3.6\ K)=S(T_K/3.6\ K)$ which yields $T_K=3.1$ K for CePtGa. This may be compared to the value $T_K^{MR}=2.4(3)$ K observed in our MR measurements. These Kondo temperature values which are in fair agreement with one another correspond to the ground state crystal field level in CePtGa. The Kondo energy scale in the higher crystal field level may be calculated from the relation $T_K^H=(T_K^L\Delta_1\Delta_2)^{1/3}$ [19]. Using the two crystal field splittings at 209 and 413 K in CePtGa that has been determined by an inelastic neutron scattering study [3] gives $T_K^H=59$ for $T_K^L=T_K^{MR}=2.4$ K. This T_K^H value is close to the higher temperature peak observed in $\rho_{mag}(T)$ of CePtGa at $T_{max}^H=67.8$ K (see Fig. 3).

Fig. 10 shows the $C_P^{mag}(T)$ data for CePtGa and the corresponding $S^{mag}(T)$ curve for temperatures up to 200 K. The $C_P^{mag}(T)$ data suggest the existence of a crystal-field excitation with a Schottky-type anomaly at 125 K. The $J=5/2$ multiplet of Ce^{3+} which occupies a site of monoclinic point symmetry in CePtGa is split

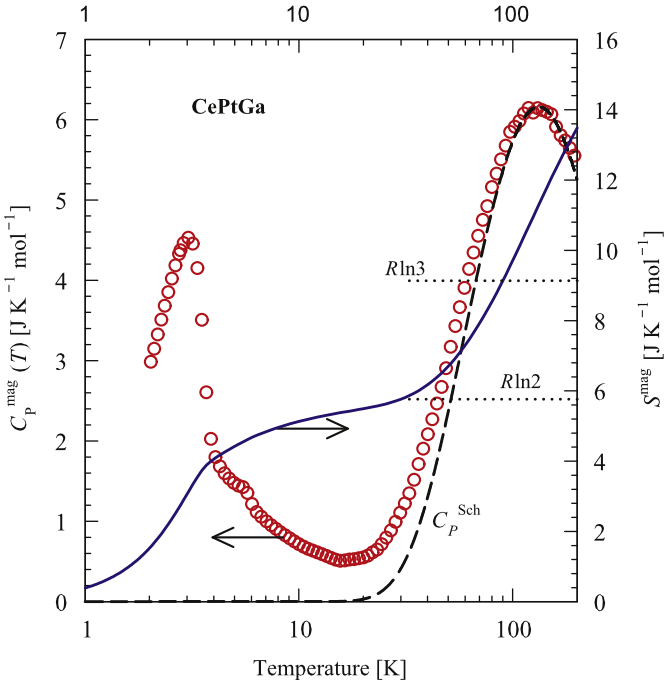

Fig. 10. The experimental $C_P^{mag}(T)$ data (open circles) is compared with the Schottky contribution C_P^{Sch} to the specific heat in accordance to Eq. (7). Also shown is the entropy $S^{mag}(T)$ of CePtGa.

into three Kramers doublets. The Schottky contribution to the heat capacity for such a three-level system may be expressed as

$$C_P^{Sch}=R\left(\frac{\Delta_1}{T}\right)^2\frac{(g_0/g_1)\exp(\Delta_1/T)}{(1+(g_0/g_1)\exp(\Delta_1/T))^2}$$

$$+R\left(\frac{\Delta_2}{T}\right)^2 \frac{(g_1/g_2)\exp(\Delta_2/T)}{(1+(g_1/g_2)\exp(\Delta_2/T))^2} \quad (7)$$

where g_0, g_1 and g_2 are the degeneracies of the three levels and R is the universal gas constant [20]. The dashed curve in Fig. 10 shows the fit to Eq. (7) that gives $\Delta_1=206$ and $\Delta_2=415$ K values with $g_0=g_1=g_2=2$. This result corroborates the inelastic neutron scattering study that indicates that the excitations are between the ground state doublet and the two excited CEF doublets at $\Delta_1=18$ (209 K) and $\Delta_2=35.6$ meV (413 K) [3]. As observed in Fig. 10, S^{mag} at $T_N=3.6$ K is about 66% of R ln 2, the value expected for a complete removal of the two-fold degeneracy of a CEF ground-state doublet. This reduced entropy value might be due to the substantial Kondo-derived reduction of the Ce moments and/or a presence of short-range correlations above T_N [21].

3.6. Volume dependence of T_N and T_K

A Doniach diagram is presented in Fig. 11 depicting the volume dependences of T_N and T_K as deduced from the present study of the solid solutions $(Ce_{1-x}La_x)PtGa$ and from previous work on the $Ce(Pt_{1-y}Ni_y)Ga$ system [7]. The results of lattice parameter measurements (see Fig. 1) were used to determine the $(V_{x=0}-V)/V_{x=0}$ values for the different samples. $T_N(x)$ values derived from $\chi(T)$ measurements in Fig. 5 are compared with $T_N(y)$ values from the earlier study. The dashed curve in Fig. 11 is a guide to the eye illustrating a maximum in the T_N values near $x=0$ and the expected vanishing of AF order near a concentration of $y\approx 0.38$. Quantum critical behaviour may be expected in this concentration region and measurements at lower temperatures are called for to investigate such a possibility. The T_K values for the $y=0.2$, 0.3 and 0.5 alloys of the $Ce(Pt_{1-y}Ni_y)Ga$ system depicted in Fig. 11 are obtained from a reanalysis of previous MR data [7] along the lines as described in Section 3.4 of the present paper. In particular in the new analysis the lower temperature isotherms are fitted in a reduced field region. The resulting $B^*(T)$ values from this analysis also deviate from linearity at low temperatures and are described by Eq. (4). Values of T_K from the present calculation are somewhat higher than previously found using a linear $B^*(T)$ dependence.

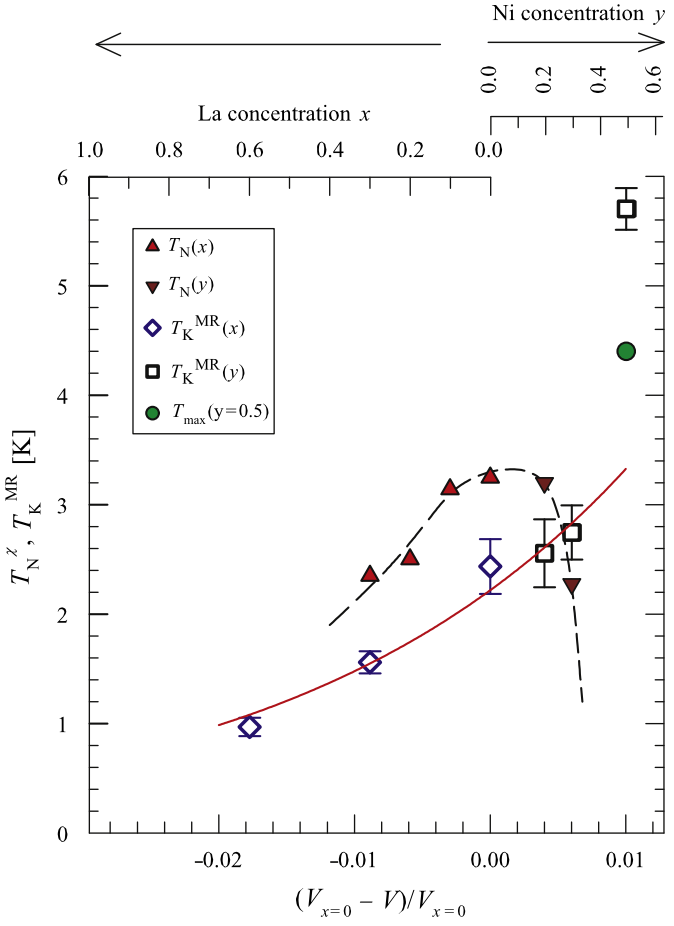

Fig. 11. A Doniach diagram for the $(Ce_{1-x}La_x)PtGa$ and $Ce(Pt_{1-y}Ni_y)Ga$ [7] systems. The Néel temperatures T_N^{χ} obtained from $\chi(T)$ measurements (Fig. 5) and the Kondo temperatures T_K^{MR} calculated from MR measurements (Fig. 7) are plotted against $(V_{x=0}-V)/V_{x=0}$ of the alloy systems. The solid curve is a LSQ fit of Eq. (8) to the T_K^{MR} data points.

The volume dependence of the T_K results depicted in Fig. 11 can be described by the compressible Kondo lattice (CKL) model [22]. This model gives the volume dependence of $|JN(E_F)|$ as $|JN(E_F)|=|JN(E_F)|_0\exp[-q(V-V_0)/V_0]$, where $|JN(E_F)|_0$ indicates the value of the quantity at an initial volume V_0. Furthermore, q refers to the Grüneisen parameter of $|JN(E_F)|$ (i.e. $q=-\partial \ln|JN(E_F)|/\partial \ln V$) and it is considered to vary between 6 and 8 [22,23]. Since $T_K\propto\exp(-1/|JN(E_F)|)$ the volume dependence of T_K may be described by

$$T_K(V)=T_K(V_{x=0})\exp\left[\frac{q(V_{x=0}-V)}{|JN(E_F)|_{x=0}V_{x=0}}\right] \quad (8)$$

as a function of the concentration dependent volume V [23,24]. The LSQ fit to Eq. (8) of the $T_K(x)$ and $T_K(y)$ values which are in the magnetic regime (shown by the solid line in Fig. 11) yield $q/|JN(E_F)|_{x=0}=41(5)$ which corresponds to $|JN(E_F)|_{x=0}=0.15(2)$ with $q=6$. As seen in Fig. 11, the T_K value at $y=0.5$ which is in the non-magnetic region deviates appreciably from the theoretical fit. This suggests that the volume dependence of T_K is different in magnetic and non-magnetic regions of our solid solution. This behaviour is furthermore illustrated in Fig. 12 which is used to calculate the Grüneisen parameter of T_K, $\Omega_K=-\partial(\ln T_K)/\partial(\ln V)$. The linear fit of $\ln T_K$ vs $\ln V$ in the antiferromagnetic region for the compositions $0\le y\le 0.3$ and $0\le x\le 0.6$ yields $\Omega_K=47(3)$. In the non-magnetic region the variation of T_K with volume is much larger leading to a value of $\Omega_K\approx 180$ calculated using the dashed

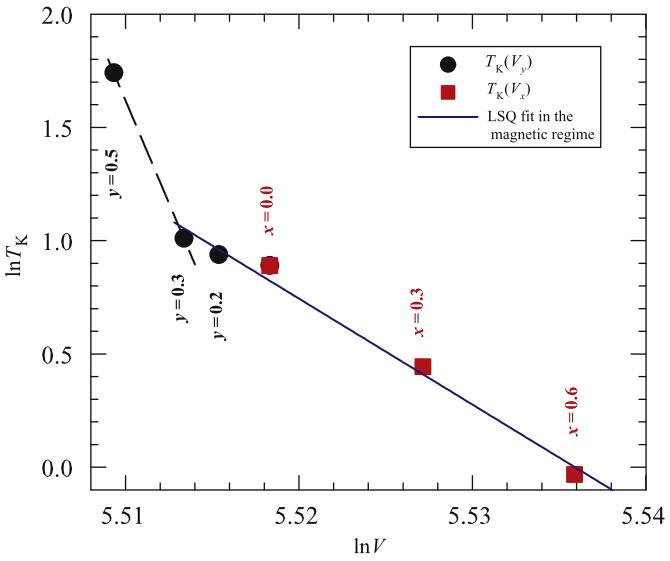

Fig. 12. The dependence of the Grüneisen parameter of T_K for the solid solutions $(Ce_{1-x}La_x)PtGa$ and $Ce(Pt_{1-y}Ni_y)Ga$ [7]. The solid line shows the LSQ linear fit in the antiferromagnetic regime and the dashed line shows the deviation at the transition to the non-magnetic regime.

line estimate in Fig. 12. Theoretically for one of the scenarios for the antiferromagnetic QCP it is expected that T_K will vanish at the QCP [25,26]. It has furthermore been indicated that the Ω_K behaviour might be different in antiferromagetic and non-magnetic regions adjacent to the QCP [26]. Clearly a study of more compositions between $y=0.3$ and 0.5 is needed to clarify the behaviour of T_K and Ω_K and compare it with theoretical expectations.

It has been observed for the $(Ce_{1-x}La_x)Pt_2Si_2$ [27] and $(Ce_{1-x}La_x)PtIn$ [28] solid solutions that the Kondo energy scale does not only depend on a volume effect as given by the CKL model but that dilution effects due to La substitution on Ce sites for Kondo hole systems [29–32] give an additional change in the Kondo energy scale. Significant deviation from the CKL model prediction observed for the $(Ce_{1-x}La_x)PtIn$ system [28] can be explained in terms of the recent model by Burdin and Fulde which considers the effects of randomness in Kondo hole systems [32]. It is however seen in Fig. 11 that the CKL model gives a fair description of the MR derived T_K values of compositions of the solid solution $(Ce_{1-x}La_x)PtGa$ which are in the magnetic regime in contrast to the above discussed T_K behaviour of the $(Ce_{1-x}La_x)Pt_2Si_2$ and $(Ce_{1-x}La_x)PtIn$ systems that are in the non-magnetic regime.

4. Conclusion

A study of the solid solution $(Ce_{1-x}La_x)PtGa$ reveals both its antiferromagnetic and Kondo characteristics. The Kondo resistivity exhibits a $(-\ln T)$ dependence in two different temperature regimes exhibiting Kondo behaviour in the crystal-field ground and excited levels. Magnetoresistance measurements are used to determine the Kondo temperature T_K corresponding to the lower crystal field ground state and fair agreement is observed with the value of T_K determined in the present study using heat capacity measurements on the CePtGa compound. The values of crystal field excitations determined using the Schottky-peak of the heat capacity conform to the reported values from an inelastic neutron scattering study. The temperature dependences of the Néel temperature T_N and the Kondo temperature T_K for the solid solution agree with the basic predictions of the Doniach diagram. The Kondo energy scale follows the compressible Kondo model in the antiferromagnetic regime. Metamagnetic behaviour is observed for CePtGa and for the $x=0.1$, 0.2 and 0.3 alloys but this behaviour disappears for larger La concentrations.

Acknowledgements

Support by the South African National Research Foundation (NRF) through Grants GUN 2053778 and GUN 2072956 and the Universities of the Witwatersrand and of Johannesburg are acknowledged. Dr. M.B. Tchoula Tchokonté is thanked for assisting with the X-ray diffraction measurements. F.C. Ragel wishes to thank the NRF and Wits University for granting bursaries for the study, and the University of Johannesburg for funding visits to its Physics Department. He also extends his appreciation to the South Eastern University of Sri Lanka for granting leave to pursue his research in South Africa.

References

[1] T. Fujita, T. Suzuki, S. Nishigori, T. Takabatake, H. Fujii, J. Sakurai, J. Magn. Magn. Mater. 108 (1992) 35.
[2] Y. Uwatoko, T. Ishii, G. Oomi, S.K. Malik, Physica B 206&207 (1995) 199.
[3] D.T. Adroja, B.D. Rainford, A.J. Neville, Physica B 223&224 (1996) 279.
[4] Y. Uwatoko, M. Kosaka, M. Shirakawa, G. Oomi, N. Môri, T. Kobayashi, H. Tatewaki, K. Shimizu, K. Amaya, Physica B 284&288 (2000) 1321.
[5] M. Shirakawa, M. Kasaya, Y. Uwatoko, G. Oomi, N. Môri, Physica B 281&282 (2000) 94.
[6] F.C. Ragel, P. de V. du Plessis, A.M. Strydom, J. Magn. Magn. Mater. 310 (2007) 365.
[7] F.C. Ragel, P. de V. du Plessis, A.M. Strydom, J. Phys.: Condens. Matter 19 (2007) 506211.
[8] E. Hovestreydt, N. Eugel, K. Klepp, B. Chabot, E. Parthé, J. Less-Common Met. 85 (1982) 247.
[9] T.J.B. Holland, S.A.T. Redfern, Mineral. Mag. 61 (1997) 65.
[10] M.B. Fontes, J.C. Trochez, B. Giordanengo, S.L. Budko, D.R. Sanchez, E.M. Baggio-Saitovitch, M.A. Continentino, Phys. Rev. B 60 (1999) 6781;
[] S.N. de Medeiros, M.A. Continentino, M.T.D. Orlando, M.B. Fontes, E.M. Baggio-Saitovitch, A. Rosch, A. Eichler, Physica B 282&282 (2000) 340.
[11] D. Kaczorowski, P. Rogl, K. Hiebl, Phys. Rev. B 54 (1996) 9891.
[12] Z. Hossain, H. Ohmoto, K. Umeo, F. Iga, T. Suzuki, T. Takabatake, N. Takamoto, K. Kindo, Phys. Rev. B 60 (1999) 10383.
[13] Z. Hossain, S. Hamashima, K. Umeo, T. Takabatake, C. Geibel, F. Steglich, Phys. Rev B 62 (2000) 8950.
[14] B. Cornut, B. Coqblin, Phys. Rev. B 5 (1972) 4541.
[15] P. Schlottmann, Z. Phys. B: Condens. Matter 51 (1983) 223.
[16] B. Batlogg, D.J. Bishop, E. Bucher, B. Golding Jr., A.P. Ramirez, Z. Fisk, J.L. Smith, H.R. Ott, J. Magn. Magn. Mater. 63&64 (1987) 441.
[17] E. Bauer, Adv. Phys. 40 (1991) 417;
[] A.M. Strydom, P.deV. du Plessis, J. Phys.: Condens. Matter 11 (1999) 2285;
[] P.deV. du Plessis, A.M. Strydom, R. Troć, T. Cichorek, C. Marucha, R.P. Gers, J. Phys.: Condens. Matter 11 (1999) 9775.
[18] H.U. Desgranges, K.D. Schotte, Phys. Lett. 91A (1982) 240;
[] H. Yashima, H. Mori, N. Sato, T. Satoh, K. Kohn, J. Magn. Magn. Mater. 31-34 (1983) 411;
[] H. Mori, H. Yashima, N. Satoh, J. Low Temp. Phys. 58 (1985) 513;
[] A.P. Pikul, D. Kaczorowski, T. Plackowski, A. Czopnik, H. Michor, E. Bauer, G. Hilscher, P. Rogl, Yu. Grin, Phys. Rev. B 67 (2003) 224417.
[19] K. Hanzawa, K. Yamada, K. Yosida, J. Magn. Magn. Mater. 47&48 (1985) 357.
[20] E.R. Gopal, in: Specific Heats at Low Temperatures, Heywood Books, London, 1966 p. 102.
[21] E. Gratz, E. Bauer, B. Barbara, S. Zemirli, F. Steglich, C.D. Bredl, W. Lieke, J. Phys. F: Met. Phys. 15 (1985) 1975 the references therein;
[] A. Braghtaa, G. Schmerbera, A. Derorya, J.G. Serenic, J.P. Kappler, J. Magn. Magn. Mater. 320 (2008) 1141.
[22] M. Lavagna, C. Lacroix, M. Cyrot, Phys. Lett. A 90 (1982) 210;
M. Lavagna, C. Lacroix, M. Cyrot, J. Phys. F: Met. Phys. 13 (1983) 1007.
[23] T. Kagayama, G. Oomi, H. Takahashi, N. Môri, Y. Ônuki, T. Komatsubara, Phys. Rev. B 44 (1991) 7690.
[24] P.deV. du Plessis, V.H. Tran, J. Phys.: Condens. Matter 9 (1997) 8527.
[25] S. Burdin, D.R. Grempel, A. Georges, Phys. Rev. B 66 (2002) 045111.
[26] L. Zhu, M. Garst, A. Rosch, Q. Si, Phys. Rev. Lett. 91 (2003) 066404.
[27] F.C. Ragel, P.deV. du Plessis, A.M. Strydom, J. Phys.: Condens. Matter 20 (2008) 055218.
[28] F.C. Ragel, P.deV. du Plessis, A.M. Strydom, J. Phys.: Condens. Matter 21 (2009) 046008.
[29] Zheng-zhong Li, Yang Qiu, Phys. Rev. B 43 (1991) 12906.
[30] S. Wermbter, K. Sabel, G. Czycholl, Phys. Rev. B 53 (1996) 2528.
[31] T. Mutou, Phys. Rev. B 64 (2001) 245102.
[32] S. Burdin, P. Fulde, Phys. Rev. B 76 (2007) 104425.